11th ANKARA INTERNATIONAL AEROSPACE CONFERENCE AIAC-2021-142
8-10 September 2021 - METU, Ankara TURKEY

NUMERICAL SIMULATION OF SPRAY CHARACTERISTICS OF DOUBLET INJECTORS

Senem Gulmez[1]
Aerospace Engineering Department
Middle East Technical University (METU)
Ankara, Turkey

Harika S. Kahveci[2]
Aerospace Engineering Department
Middle East Technical University (METU)
Ankara, Turkey

ABSTRACT

Spray characteristics of impinging jets have been widely studied over the years to improve atomization and mixing of jets that considerably affect combustion efficiency, especially in liquid-propellant rocket engines. In this study, numerical simulations of two impinging jets are performed using ANSYS Fluent with the Coupled Level Set and Volume of Fluid (CLSVOF) method and the Adaptive Mesh Refinement (AMR) technique. The computational methodology is validated using two sets of experimental data from literature. Among the investigated are the mesh size required for resolving the spray characteristics such as the liquid sheet breakup and surface waves, the velocity distributions along the impingement and stagnation lines, and the droplet statistics of the spray. Results show that the atomization process of impinging jets can be analyzed with reasonable accuracy with the method used.

INTRODUCTION

In liquid-propellant rocket engines, the injector is one of the most important components of the thrust chamber that supports achieving a stable and efficient combustion process. The main objective of the injector design is to supply the fuel and oxidizer at predefined proportions so that the reaction between the two gives the highest energy level possible. In addition to this, the pressure drop due to injectors increases the stability of the engine. Liquid-propellant rocket engine injectors are categorized in three groups as straight injectors, centrifugal injectors, and coaxial injectors [Wang, 2016]. The straight injectors are subcategorized as impinging and non-impinging. Doublets are one of the commonly used impinging injectors. They are used in many rocket engines such as the F-1 engine in Saturn, the A-7 engine in Redstone, and the booster and stage 2 engines in Titan 1 [Gill, Nurick, Keller, and Douglass, 1976]. In doublets, liquid streams impinge directly on each other. At the impingement point, a liquid sheet spray is produced and the resultant spray grows in the axial direction. In the case that both injector elements impinge the same type of propellant, the injector type is called a like-doublet injector. Like-doublets are good at maintaining combustion stability and preventing reactive-stream demixing [Huzel and Huang, 1992]. Despite these advantages, compared to the unlike-doublets with elements having different kinds of reactants, the like-doublets are not good at initial mixing. On the other hand, the unlike-doublets, in general, do not form an axial fan due to different momenta of liquid jets.

[1] M.Sc. Student in Aerospace Engineering Department, METU, Email: gulmez.senem@metu.edu.tr
[2] Assoc. Prof. in Aerospace Engineering Department, METU, Email: kahveci@metu.edu.tr

As a solution to this problem, triplet and pentad injectors can be used, where two outer orifices of the triplet and four outer orifices of the pentad injectors impinge on the center orifice. In general, the outer orifices are designed to inject oxidizer and the center orifice injects fuel considering the high mixture ratio of propellant combinations. The spray characteristics such as droplet statistics, liquid wave, spray breakup length, and spray distribution are directly related to the injector element, therefore, these properties should be analyzed for the selected type of the injection element.

Several spray atomization studies have been carried out both experimentally and numerically. Since the current study focuses on doublet injectors, the research summarized here is confined to those that also studied the same type of injectors. Ryan et al. [Ryan, Anderson, Pal, and Santoro, 1995] investigated the effects of flow properties and injector geometric parameters on the droplet diameter, sheet breakup length and surface wave of like-doublet injectors. Breakup length and wave results were obtained from images taken by a high-speed camera. Velocity and diameter of the droplets were measured by the Phase Doppler Particle Analyzer (PDPA).

Lai et al. [Lai, Huang, and Chu, 2004] performed an experimental study on spray characteristics such as the spray pattern, mean droplet size and mixture ratio of an unlike-doublet impinging-jet at different jet velocities. A high-speed camera and a stroboscope were used to visualize the sprays, while the spray distribution was obtained by a patternator, and a laser diffraction sizing device was used to obtain the mean droplet size. It was concluded that the unlike-doublet spray pattern had a similarity to those of like-doublet ones. The droplet sizes were found to decrease with an increase in the velocity of the fluid jets. Also, the variation of the deviation angle of the resultant spray with the mixture ratio and the mass flow rate ratio agreed well with the theoretical calculations.

Arienti et al. [Arienti, Li, Soteriou, Eckett, Sussman, and Jensen, 2013] developed a numerical method to simulate the breakup and atomization of a liquid flow by using the Coupled Level Set and Volume of Fluid (CLSVOF) with the Adaptive Mesh Refinement (AMR) technique. They used the experimental data of Ryan et al. [Ryan, Anderson, Pal, and Santoro, 1995] obtained at different jet velocities for comparisons. They also compared the particle density distribution of different refinement levels with the experimental data provided by Anderson et al. [Anderson, Ryan, Santoro, and Hewitt, 1995]. Results indicated that the use of intermediate and fine meshes improved the computational accuracy compared to the coarse mesh.

Chen et al. [Chen, Ma, and Yang, 2012] performed a numerical study for the formation and breakup of impinging jets at different Reynolds and Weber numbers by using the Volume of Fluid (VOF) method with AMR. They obtained good agreement between the numerical and the experimental results of Ryan et al. [Ryan, Anderson, Pal, and Santoro, 1995].

Another study was conducted by Zheng et al. [Zheng, Nie, Feng, and Wu, 2015] to analyze the influence of the impingement angle on two like-doublet configurations experimentally, and the results were compared with numerical findings. They used the CLSVOF method in order to capture the interface between the liquid and the gas. The evaluation criterion was selected as the Sauter Mean Diameter (SMD). The findings indicated that the SMD values from both experiments and numerical results decreased slightly when the impingement angle was increased. However, the numerical results had a percentage difference varying between 11% and 35% compared to the experimental results at two impingement angles.

Balasubramanian et al. [Balasubramanian, Kumar, Nakod, Schütze, and Rajan, 2020] analyzed the break-up mechanism and particle distribution of the doublet injector case studied by Zheng et al. [Zheng, Nie, Feng, and Wu, 2015] by using the coupled VOF and Discrete Phase Model (DPM) with the AMR technique that can refine the cell size up to 20 μm. It was seen that the velocity magnitudes obtained along the spray centerlines for the two impingement angles were calculated differently by this numerical method compared to the method used by Zheng et al. [Zheng, Nie, Feng, and Wu, 2015].

In this study, numerical analyses are conducted to investigate the necessary mesh size in order to capture the spray characteristics such as the liquid sheet breakup, surface wave,

and droplet diameter. Two sets of computations are pursued to validate the computational methodology. In the first validation study, the computed SMD results are compared with the experimental data provided by Zheng et al [Zheng, Nie, Feng, and Wu, 2015], whereas the liquid sheet characteristics and velocity distributions obtained by both Zheng et al. [Zheng, Nie, Feng, and Wu, 2015] and Balasubramanian et al. [Balasubramanian, Kumar, Nakod, Schütze, and Rajan, 2020] are used for additional numerical comparisons. The second validation study uses the experimental data of Anderson et al. [Anderson, Ryan, Santoro, and Hewitt, 1995] and compares the computed number distribution of drop sizes in the spray.

COMPUTATIONAL METHODOLOGY

In this section, the computational approach undertaken for the analyses is described. The computational domain, mesh sensitivity and comparisons performed for the two validation studies are presented in detail.

Validation Case 1

In order to perform the aforementioned comparisons, a model similar to the one used in the study of Zheng et al. [Zheng, Nie, Feng, and Wu, 2015] is generated using the same geometric dimensions and boundary conditions. The schematic of the cross-section of the resultant spray in the computational domain is given in Figure 1. Water is used as the working fluid in a like-doublet injector with an impingement angle, 2α, of 80°. Density and viscosity of the water are defined as 998.2 kg/m^3 and 0.001003 kg/ms in Fluent, respectively. The surface tension between water and air is defined as 0.0725 N/m. Mean Re is calculated as 25389 and We as 8960, respectively. A mass flow rate, $\dot{m}_i$, of 0.020 kg/s is supplied at the inlet of each orifice having a diameter, d_o, of 1 mm, at a turbulence intensity of 5%. The pre-impingement length, L_{imp}, is defined as 5 mm. The surface normals of the inlet and exit of the orifices are modeled to be perpendicular to the volume that the liquid jets are injected into, so that a normal velocity distribution along the orifices and a realistic liquid jet behavior with droplet formation at the exit of the orifices can be established. The domain is filled with air, and the ambient pressure boundary condition of 1 atm is assigned to the outlet to match the case study. All boundary surfaces other than the inlets and orifice walls are defined as the outlet as shown in Figure 1. Wall boundary condition is applied along the orifices.

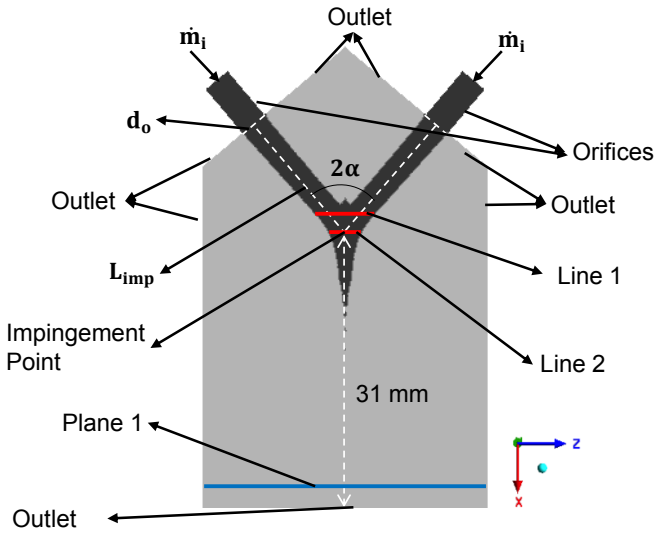

Figure1: Cross-Section of the Computational Domain Used in Validation 1 (not to scale)

The SMD measurements are performed at Plane 1, which is 30 mm away from the impingement point. Line 1 passes through the stagnation point along the z-axis and Line 2 is parallel to Line 1 and passes through the impingement point that is also the origin of the domain. In current study, the stagnation point was defined as the point that has the highest

local pressure inside the impact region of liquid jets. This location was found to be varying between 0.65 mm and 1 mm above the impingement point among the studied cases. Zheng et al. [Zheng, Nie, Feng, and Wu, 2015] presents results along the line through the stagnation point as well, but with no information on its location. The computational domain is 37.5 mm x 24 mm x 10 mm in x, y and z directions, respectively. Because of the highly three-dimensional behavior of spray atomization, a three-dimensional analysis is conducted.

Computations are performed with ANSYS Fluent v17.0 by using the CLSVOF method with the AMR technique. CLSVOF combines the benefits of the VOF method of mass conservation and the Level Set (LS) method of capturing the liquid-gas interface. The detailed mechanism is explained in the study of Sussman et. al. [Sussman, Smith, Hussaini, Ohta, and Zhi-Wei, 2007]. The k-ω SST model effectively brings together the advantages of the k-ω model at the near-wall region and k-ε model in free-stream [Wang, 2016]. Hence, since the current study involves both flow through orifices and free-stream, the k-ω SST is chosen as the turbulence model. The curvature method with gradient of fluid volume fraction is used for mesh refinement and the variable time stepping method is enabled with a global Courant number of 2.

Use of Adaptive Mesh Refinement (AMR)

A three-level adaptive mesh is used in the liquid volume for all analyses. The minimum cell sizes of 100, 80, 60, 50, 40 and 30 μm were achieved in the analyses of M1, M2, M3, M4, M5 and M6, respectively. The orifice domains were further resolved with the minimum cell size mentioned at each analysis so that the velocity profile of the liquid jet could be captured at the exit of the orifices. Inner iterations were repeated until the mass, momentum, k-ω and LS function residuals were reduced to level of around 0.001. Cases had different total run times. The initial number of nodes and the final number of nodes at t=1.6 ms, which corresponds to a time after the first droplet reaches the bottom of the domain, are given in Table 1 for each case. Table 1 also shows the equivalent number of nodes that would be required in a uniform mesh using the minimum cell size if the adaptive mesh technique was not used. The comparison of the two mesh types shows that the number of nodes required for the coarsest uniform mesh is higher even than that required for the finest adaptive mesh. Besides, the difference in the number of nodes between adaptive mesh and uniform mesh increases drastically as the minimum cell size is further decreased. This shows that the adaptive mesh refinement makes the atomization simulations affordable in terms of computational costs.

Table 1. Number of Nodes for Each Case Used in Mesh Sensitivity for Validation 1

	M1	**M2**	**M3**	**M4**	**M5**	**M6**
Minimum Cell Size	100 μm	80 μm	60 μm	50 μm	40 μm	30 μm
Initial Number of Nodes - AMR	34426	58812	133270	213906	393278	886660
Final Number of Nodes - AMR	887109	1415936	2627055	3759786	6652385	11329490
Total Number of Nodes - Uniform Mesh	12218430	23652066	55616960	95930796	187326376	441557132

In Figure 2, the fluid volumes of water are given at a cross-section of the domain along the direction of the flow. Cells with a volume of fraction of 1 include only water. All values other than 1 indicate the cells where water and air coexist. Each volume shows the mesh for each analysis at the time of 1.6 milliseconds as repetitive liquid sheet breakups are acquired. A blow-up view of the water-air interface is given in Figure 3 for cases M5 and M6. In the vicinity of this region, it can be seen that the cell sizes become smaller and merge at the center of the spray reducing the overall number of nodes. As the minimum cell size decreases from M1 to M6, the interface between water and air is further resolved and the symmetrical behavior of the liquid sheet across the domain vanishes. Due to the impact of

the two liquid jets, the mixing of these jets propagates in both axial and lateral directions until the formed liquid sheet breaks into ligaments due to the formation of the surface waves, resulting in a thin liquid sheet below the impingement point. Cases M1 and M2 cannot

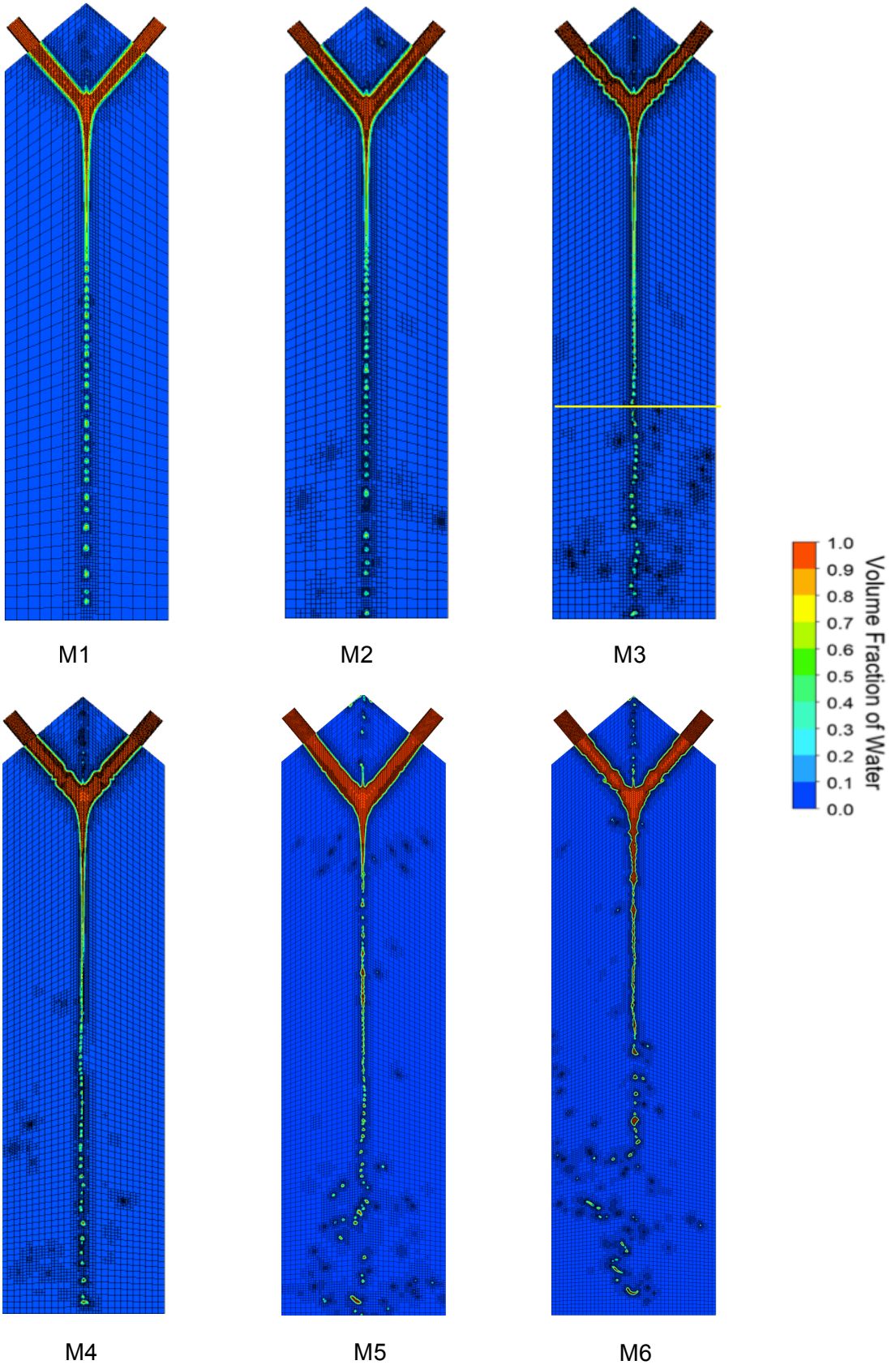

Figure 2: Cross-Section of the Fluid Volumes With Meshes at t=1.6 ms in Validation 1

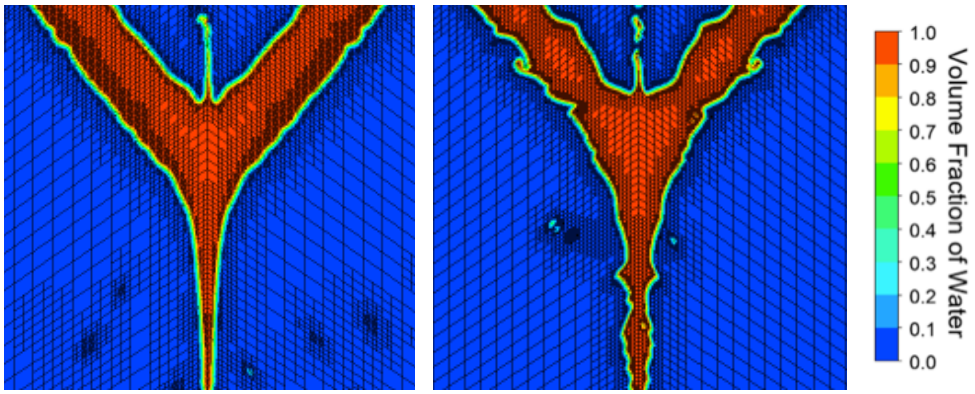

M5 M6

Figure 3: Blow-up View of Adapted Cells in M5 and M6 at t=1.6 ms in Validation 1

resolve the liquid sheet well enough to capture the fluctuations on the surface of the sheet. Those fluctuations are observed at 20 mm downstream of the impingement point for the first time in case M3 as shown in Figure 2 with the horizontal line, and are also captured by the other cases with smaller cell sizes.

The range of minimum cell sizes used in this study was considered by taking into account the other findings in the literature. Zheng et al. [Zheng, Nie, Feng and Wu, 2015] modeled a fluid volume with dimensions of 35 mm x 24 mm x 10 mm and used 2.1 million mesh cells with a minimum cell size of 40 μm. Balasubramanian et al. [Balasubramanian, Kumar, Nakod, Schütze, and Rajan, 2020] resolved a similar domain with a radius of 24 mm and a length of 35 mm with 800000 cells and used the adaptive mesh refinement with a minimum cell size of 40 μm until 3 ms, applying further refinement to reduce the minimum cell size to 20 μm for the rest of the analysis. In another study, Chen et al. [Chen, Ma, and Yang, 2012] used the adaptive mesh technique with three refinement levels with minimum cell sizes of 80, 40 and 20 μm. Arienti et al. [Arienti, Li, Soteriou, Eckett, Sussman, and Jensen, 2013] also used the AMR technique to resolve a fluid domain of 12 mm x 16 mm x 24 mm enabling three refinement levels. Considering almost the half size of the domain used by Zheng et al. [Zheng, Nie, Feng and Wu, 2015] mentioned above and the simplified orifice geometry in order to reduce the overall computational cost, the minimum cell sizes of 62.5 μm, 31.25 μm and 15.625 μm could be studied. In the current study, the full-scale domain of 37.5 mm x 24 mm x 10 mm is modeled in all analyses to capture the asymmetric nature of the problem. Hence, due to limited computational resources and costs, minimum cell sizes smaller than shown in Table 1 were not studied. As given in Table 1, the case with the minimum cell size of 30 μm (M6) reaches the number of nodes of 11.3 millions with adaptive mesh at t=1.6 ms, while this number is only 6.6 millions for the case with 40 μm cell size (M5). Besides, the average percentage of differences in the predicted velocity magnitudes along Line 2 is calculated as 18.1% between M4 (50 μm cell size) and M5. This reduced to 4.7% between M5 and M6. Comparisons of these cases with available data from literature will be presented in the following sections. Considering the close agreement of the results from cases M5 and M6, it is apparent that the selection of case M5 will bring the benefits of significantly lower computational costs compared to the latter.

General Spray Characteristics

Figure 4 shows the snapshots of the isosurfaces of volume fraction of liquid phase for each case. As described by Balasubramanian et al. [Balasubramanian, Kumar, Nakod, Schütze, and Rajan, 2020], the liquid sheet thickness varies due to the surface waves, forming holes at the thinner parts of the liquid stream. These holes expand in both lateral and axial

directions due to the velocity difference in the liquid sheet and form ligaments. In a similar manner, ligaments break up into small droplets. The core region of the liquid sheet is obtained in all cases as shown in Figure 4, however, the details of the break-up mechanism such as the surface waves forming due to the impact of liquid jets and the liquid sheet deformation into ligaments are not resolved in the core region as much as in M5 and M6.

In their computations, Zheng et al. [Zheng, Nie, Feng, and Wu, 2015] used a fixed mesh of 2.1 million cells with a minimum cell size of 40 μm and performed their analysis up to around 1.3 ms. On the other hand, Balasubramanian et al. [Balasubramanian, Kumar, Nakod, Schütze, and Rajan, 2020] used an adaptive mesh as done in the current study, while further reducing the minimum cell size to 20 μm and performing the analysis up to 5 ms.

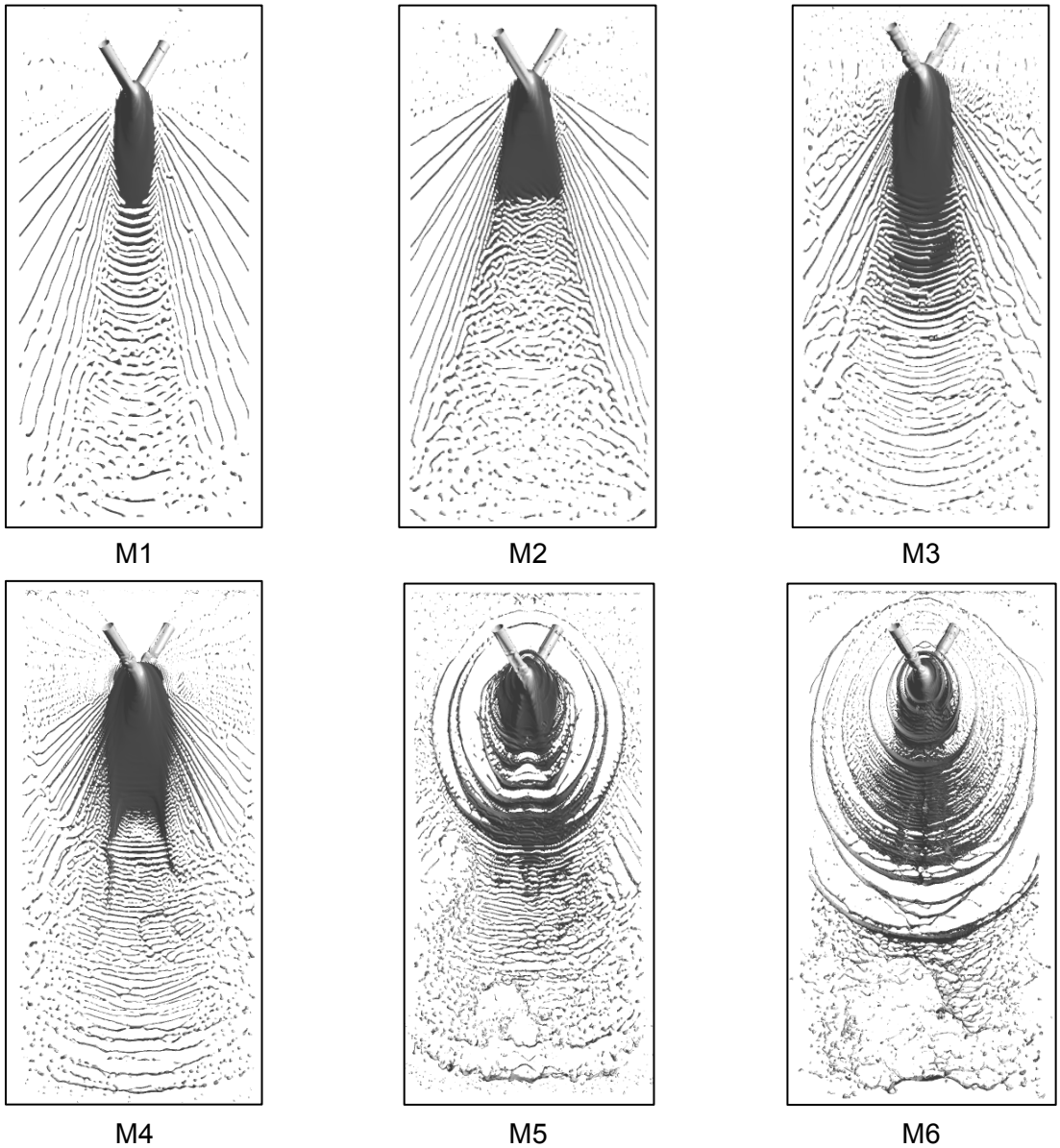

Figure 4: Comparison of Snapshots of Sprays at t=1.6 ms

The break-up length in current cases cannot be compared to the results of the experiment performed by Zheng et al. [Zheng, Nie, Feng, and Wu, 2015] since quantitative data were not provided. Their numerical results indicate the existence of large droplets both in the vicinity of the impingement location and across the computational domain, which does not agree with neither the current findings nor those of Balasubramaniyan et al. [Balasubramanian, Kumar, Nakod, Schütze, and Rajan, 2020]. This could be due to the relatively coarse mesh that was

adopted by Zheng et al. [Zheng, Nie, Feng, and Wu, 2015]. On the other hand, when the given spray snapshots of M5 and M6 are visually examined, more similarities to the results obtained by Balasubramanian et al. [Balasubramanian, Kumar, Nakod, Schütze, and Rajan, 2020] are observed in terms of break-up length and droplet density in the vicinity of the liquid core region.

Snapshots of Spray View by Simulation M5 With Respect to Time

Simulation M5 is selected to demonstrate the evolution of spray with respect to time for further insight. The snapshots at each time interval are given in Figure 5.

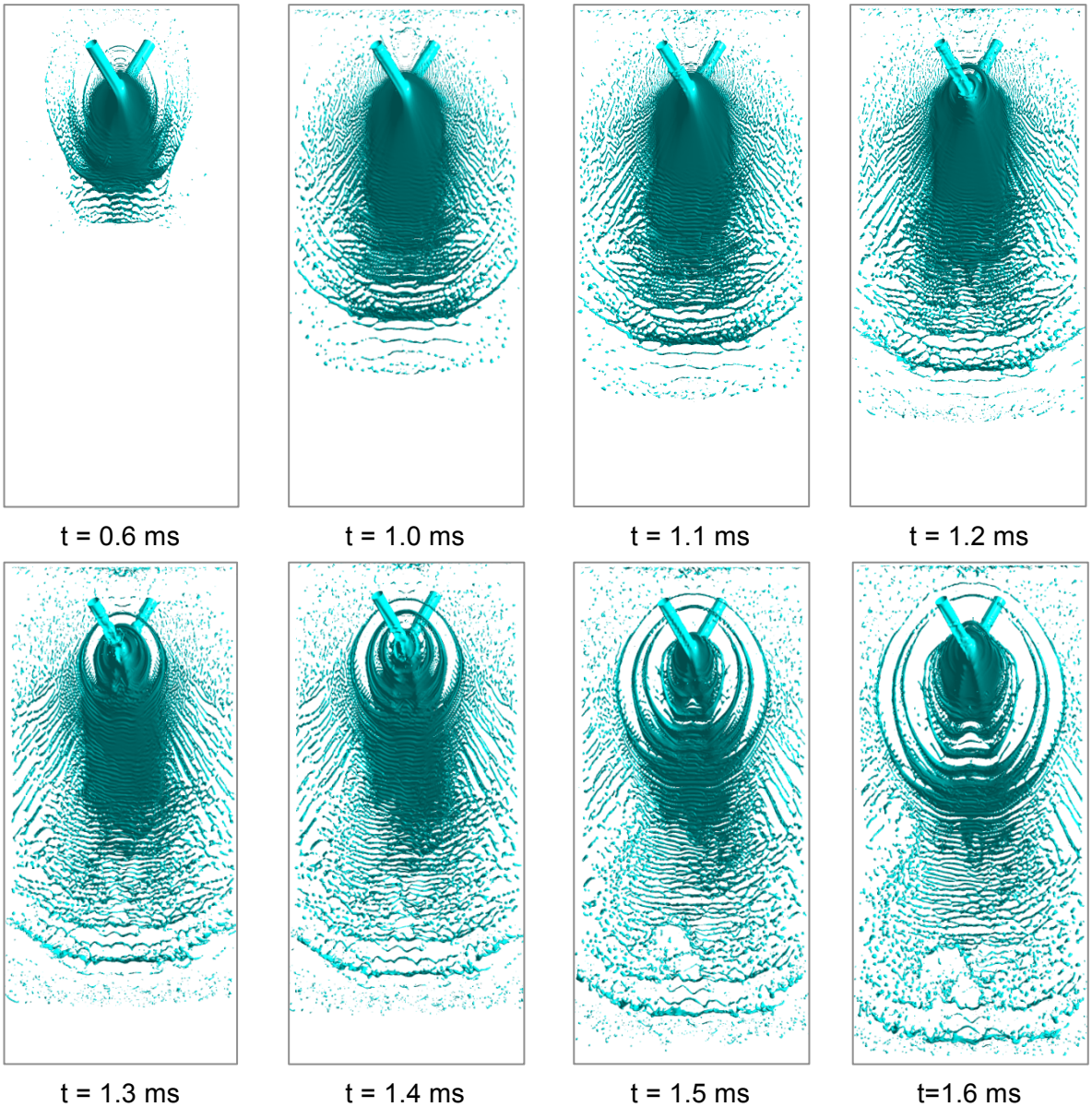

Figure 5: Spray View with Respect to Time (M5)

Fluctuations in the liquid core and small droplets exist even at 0.6 ms. The first liquid sheet break up becomes observable at 1 ms. The liquid sheet length increases until 1.2 ms without a major change in the spray structure. The initial hole that forms surrounding the vicinity of the impingement point at 1.2 ms enlarges and triggers the surface waves as can be seen at 1.3 ms. Beyond this instant in time, additional holes are observed to be forming with time. Fluctuations on the liquid sheet due to these surface waves cause the liquid sheet to break up into more ligaments at 1.5 ms. After that, the successive break up of the liquid sheet keeps progressing at 1.6 ms as a result of the formation of additional holes.

Comparison of Droplet Size

Droplets passing through Plane 1 are used in comparison of the SMD calculations. The studies of Zheng et al. [Zheng, Nie, Feng, and Wu, 2015] and Balasubramanian et al. [Balasubramanian, Kumar, Nakod, Schütze, and Rajan, 2020] will be referred to as Study 1 and Study 2, respectively, hereafter for simplicity. It should be noted that there are unfortunately limited experimental data that could be used in the validation of current computations.

Table 2: Comparison of SMD Results With Study 1 [Zheng, Nie, Feng, and Wu, 2015] and Study 2 [Balasubramanian, Kumar, Nakod, Schütze, and Rajan, 2020]

Distance from impingement point (mm)		Study 1 (Exp.)	Study 1 (Num.)	Study 2 (Num.)	M5 (Current Study)	M6 (Current Study)
10	**SMD (μm)**	129	147.1	144	135	143
	Difference (%)		14	11.6	4.3	10.8
20	**SMD (μm)**	125	149.2	147	162	111
	Difference (%)		19.4	17.6	29.7	10.8
30	**SMD (μm)**	127	140.9	182	143	139
	Difference (%)		10.9	43.3	12.6	9.4

Table 2 presents the values from both studies along with the results from cases M5 and M6 of the current study. All percentage differences given are calculated with respect to the experimental data of Study 1. Study 1 also provides a statistically averaged numerical value for the SMD over different time instants, which has a difference of 10.9% from the measured value at 30 mm. The authors attribute these differences to the reasons such as omitting the flow development inside the injectors in their computations, measurement errors, and limited grid resolution. In the current study, an average SMD was calculated using different time intervals until the end of an analysis. Good agreement on the SMD results are observed for both cases of M5 and M6 at 30 mm with a difference of only 1.5% and 1.3% from the numerical results of Study 1, and with a difference of 12.6% and 9.4% from the experimental value for each case, respectively. On the other hand, although the liquid sheet characteristics of current simulations of M5 and M6 were found to be in agreement with Study 2, a larger deviation is observed here with Study 2 in the SMD results. This can be explained to be due to the use of the VOF-DPM method in that study, as the authors explain. In this method, since the droplets are tracked with DPM, the ligaments and droplets are transported from the VOF domain to the DPM domain when the predefined conditions are reached, which may lead to a loss in the droplet count or to a change in the droplet diameter. The authors also mention the uncertainty that might be caused by the mesh selection that was driven by limited resources. Also it should be noted that, in contrary to Study 1, in the current study, a distinct atomization zone could not be observed at 10 mm and 20 mm below the impingement point since the computational domain was mainly filled by ligaments at those locations and there was considerably a much smaller number of droplets compared to those found at 30 mm distance.

In Figure 6, the droplet size distribution of M5 and M6 are given on a probability density scale. The analysis with M5 provides a normal diameter distribution according to the Anderson-Darling goodness-of-fit hypothesis test with a p-value of 0.063. The mean diameter (D10) is 119.2 μm with a standart deviation of 39.9 μm. This value reduces by 10% to 107.8 μm in M6, and the standart deviation increases by 5 μm with a p-value of 0.068. In other words, the minimum mesh cell sizes of 40 μm and 30 μm give compatible results, as will be also demonstrated in the velocity comparisons in the next section.

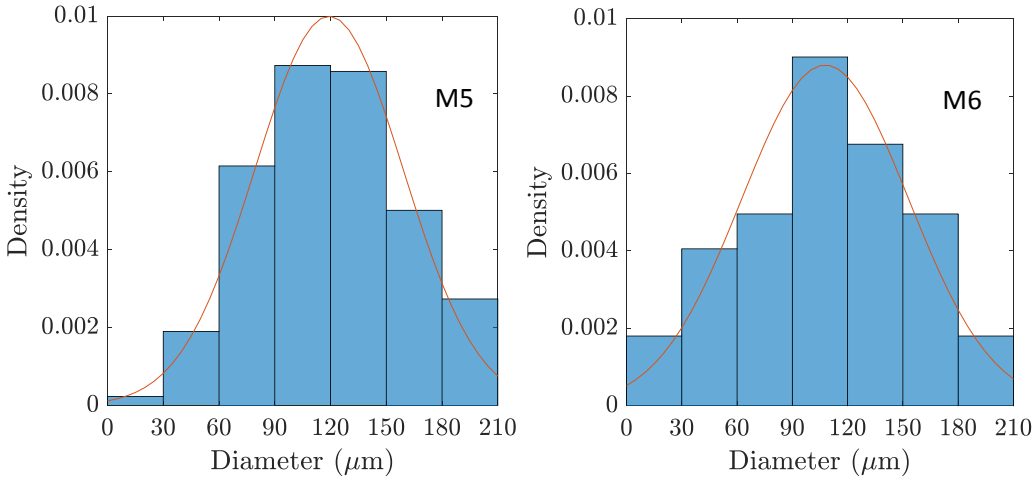

Figure 6: Droplet Size Distributions With M5 and M6

Comparison of Velocity Distributions

Figure 7 shows the velocity distributions along Line 1 and Line 2 that were denoted in Figure 1. Both of these lines reside inside the liquid volume, with Line 1 having a length of 2 mm and Line 2 a length of 1.3 mm. Figure 7a shows the distribution of the velocity magnitude along the line passing through the stagnation point, Line 1, which has the highest local pressure in the liquid sheet. As mentioned before, this line passes through approximately 1 mm above the impingement point in the current study, but it should be noted that this value in Study 1 is not known. In Figure 7a, results from all cases in the current study are somewhat in agreement with Study 1 at the center. However, the discrepancy between Study 1 and the cases M5 and M6 draw apart away from the center. This is also observed in the comparison of the z-component of the velocity along Line 1 given in Figure 7b. The coarse meshes give a very close result to that of Study 1. This is not unexpected considering the relatively coarse mesh used in the mentioned study. In both comparisons, M5 and M6 show very close velocity distributions to one another along the line. Figure 7c and Figure 7d present the velocity magnitude and the velocity component in z direction along Line 2, which passes through the impingement point. Due to the impact of the two jets, the velocity magnitude decreases around the impingement point staying between 22 and 25 m/s around the center for all cases, but differences between them become more apparent away from the center. It seems that the velocity magnitude distributions predicted by current analyses are in better agreement with Study 2 than with Study 1, while Study 1 does not seem to properly capture the general trends. M5 differs by 8.8% on average from Study 2, while this value is reduced by half with M6. On the other hand, unlike the velocity magnitude distribution, the velocity component in z direction for all cases agree with those from both of the studies with a maximum deviation of 5 m/s. Velocity in the z direction is almost equal to zero at the center, which seems to be underpredicted by Study 2, and increases further away from the center. Since there is no experimental data available for velocity distributions, the deviations among current computations and these reference studies are considered to be a result of the differences in the meshes, methods, and the turbulence models used in those studies. Although the CLSVOF method was used in Study 1 [Zheng, Nie, Feng, and Wu, 2015] similar to the current study, the AMR was not applied. The total number of mesh cells used was 2.1 millions, which is much less than the corresponding number of mesh cells of 4.9 and 8.4 millions for M5 and M6 used in this study, respectively, with the use of AMR. There is also no information provided on the turbulence model used in that study. On the other hand, in Study 2 [Balasubramanian, Kumar, Nakod, Schütze, and Rajan, 2020], the VOF-DPM method with the AMR is used for the analysis that had a minimum cell size of 20 μm, and a hybrid Reynolds-Averaged Navier-Stokes (RANS) with Large Eddy Simulation (LES) turbulence model was implemented. Despite all these discrepancies, these findings present additional insight and provide useful data to be used in comparisons in future studies.

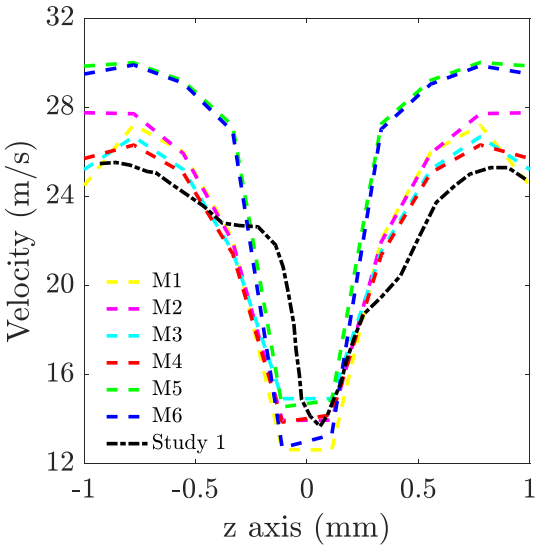

a) Velocity Magnitude Along Line 1

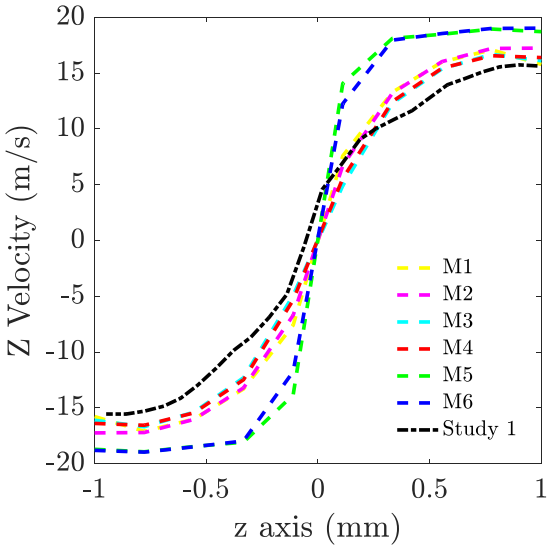

b) Z-Component of Velocity Along Line 1

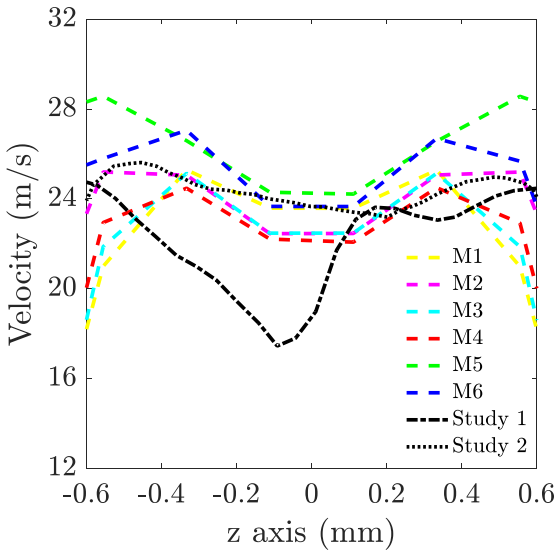

c) Velocity Magnitude Along Line 2

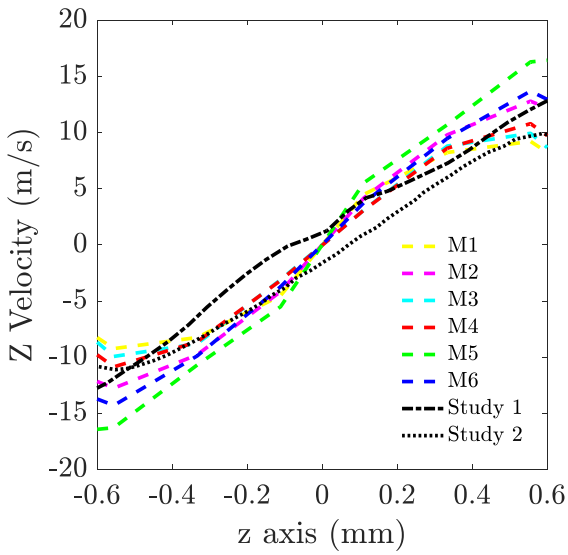

d) Z-Component of Velocity Along Line 2

Figure 7: Comparison of Velocity Distributions With Study 1 [Zheng, Nie, Feng, and Wu, 2015] and Study 2 [Balasubramanian, Kumar, Nakod, Schütze, and Rajan, 2020]

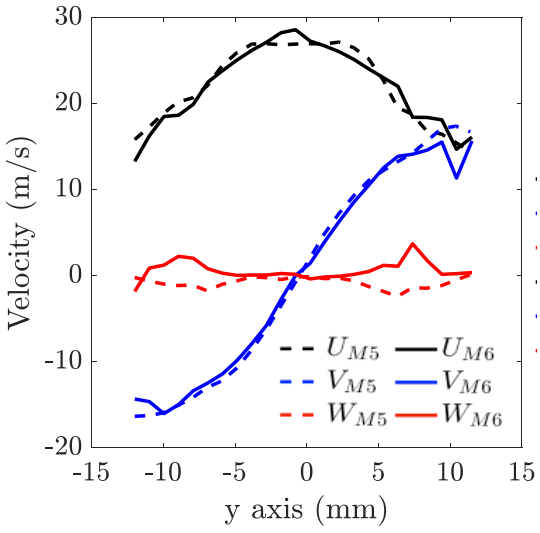

Figure 8: Comparison of Velocity Distributions at x=20 mm With M5 and M6

In Figure 8, the comparison of velocity variation inside the liquid sheet at 20 mm below the impingement point along y-axis is given. U, V, and W are the velocity components in x, y, and z directions, respectively. Similar trends are observed for velocity distributions in both cases. The average percentage of difference between the two is 5.2% for the U component, and is calculated as 13.5% for the V component due to lower velocity levels observed.

Validation Case 2

For this case, another computational domain is modeled that resembles that of the first validation case, but reflects the geometric dimensions used in the experiments of Anderson et al. [Anderson, Ryan, Santoro, and Hewitt, 1995]. It has an orifice diameter of 0.635 mm, a pre-impingement length of 25.4 mm, an orifice length-to-diameter ratio of 80, and an impingement angle of 60°. The distance from the impingement point to the bottom of the domain is 28 mm. The height of the meshed volume is 57 mm from tip to bottom, and extends by 30 mm in lateral directions. Including the full length of the orifices, the overall dimensions of the computational domain becomes 77 mm x 95 mm x 30 mm in x, y, and z directions, respectively. The working fluid in this case is also water. Instead of mass flow rate, a jet velocity of 18.5 m/s is defined at each orifice inlet in order to match the experimental test setup. Computations are performed with the same methods and techniques described in the first validation case.

Use of Adaptive Mesh Refinement (AMR)

A five-level adaptive mesh is used in the liquid volume for all analyses. This time, taking into account the findings of the previous study, the mesh sensitivity study is limited to three minimum cell sizes, being 50, 40, and 30 μm denoted by the analyses M4, M5, and M6, respectively, to be consistent with the nomenclature used in the first validation.

Table 3: Number of Nodes for Each Case Used in Mesh Sensitivity for Validation 2

	M4	M5	M6
Minimum Cell Size	50 μm	40 μm	30 μm
Initial Number of Nodes - AMR	678885	1232235	2504172
Final Number of Nodes - AMR	2037678	2948089	6821037
Total Number of Nodes - Uniform Mesh	479684966	934007872	2213867670

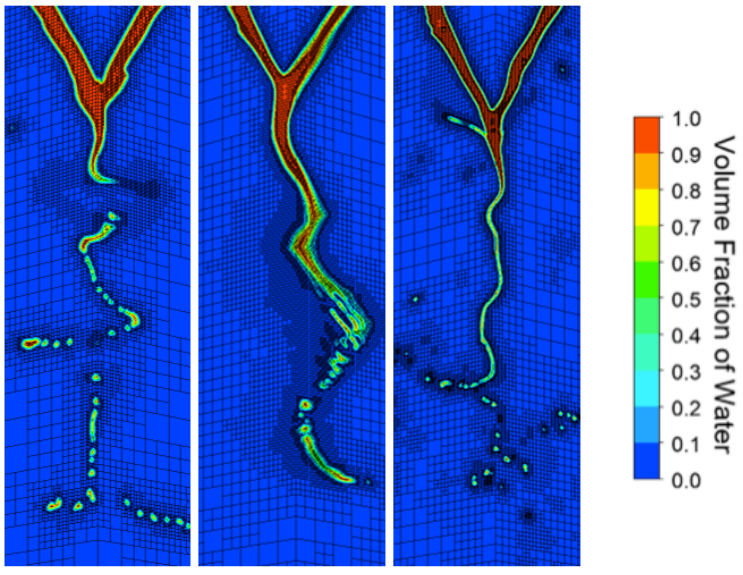

M4 M5 M6

Figure 9: Blow-up View of Cross-Section of the Fluid Volumes With Meshes at t=4.5 ms in Validation 2

The initial number of nodes and the final number of nodes at t=4.5 ms is given in Table 3 for each case. An equivalent number of nodes that would be required with a uniform mesh using the minimum cell size is also provided. Comparing the number of nodes for the intermediate mesh (M5) and the fine mesh (M6), a significant reduction is obvious. In the same manner, inner iterations were repeated until the mass, momentum, k-ω and LS function residuals were reduced to level of around 0.001. The average percentage of differences in the predicted velocity magnitudes along the spray centerline in x direction is calculated as 3.5% between M4 and M5, and 6.1% between M5 and M6 given the larger difference between these two mesh sizes. Figure 9 shows the blown-up cross-sectional views of all three meshes at the time of t=4.5 ms.

Comparison of Droplet Size

Experimental data used in the comparison given in Figure 10 were obtained by Anderson et al. [Anderson, Ryan, Santoro, and Hewitt, 1995] along the spray centerline at 41 mm downstream of the impingement point. The droplet size was measured in terms of the arithmetic mean diameter (D10). Since the distance between the impingement point and the bottom of the domain in the current study is 28 mm, the results are collected at a plane 16 mm downstream of the impingement point instead. Arienti et al. [Arienti, Li, Soteriou, Eckett, Sussman, and Jensen, 2013] performed a similar comparison with the same experimental data at the same locations, and stated that the time-averaged diameter distributions do not change between the two planes. Hence, the droplet size distribution of D10 is compared with the computation results as given in Figure 10, where the histogram bars show the result of each analysis and the orange curve shows the experimental data. In agreement with the

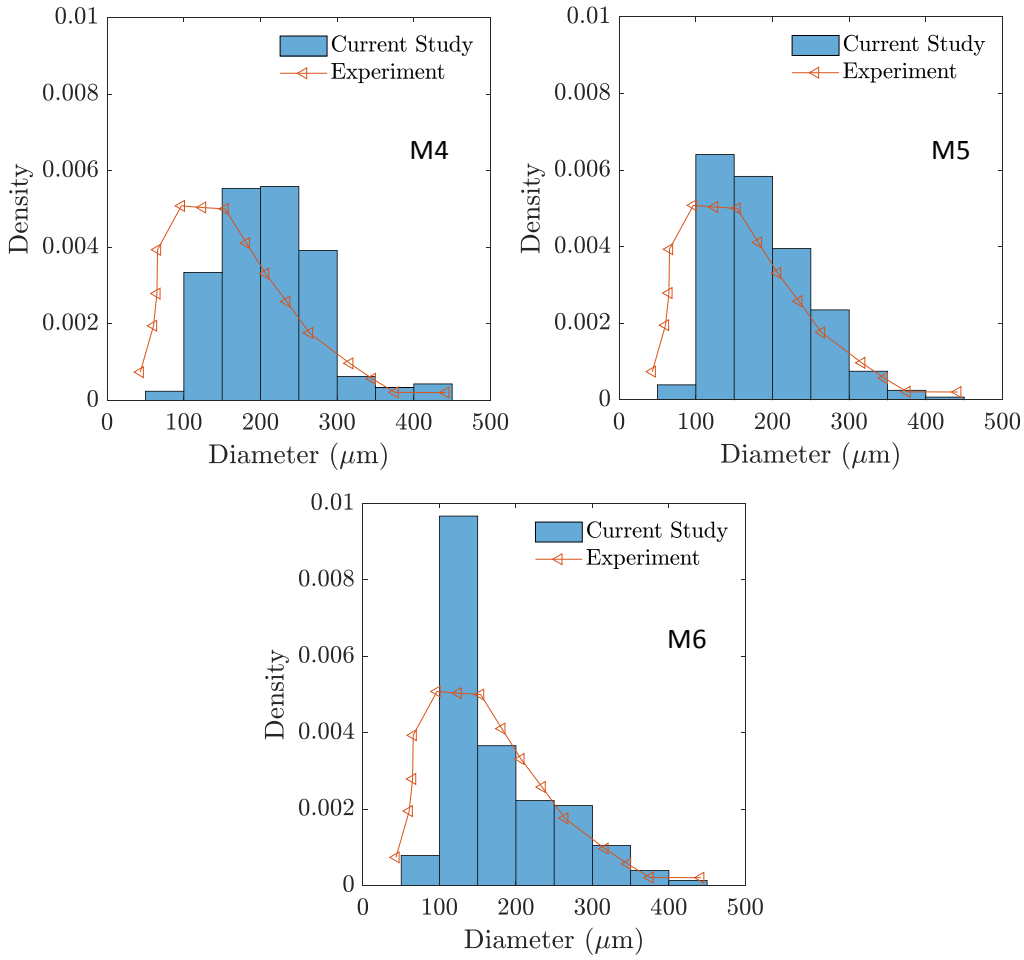

Figure 10: Comparison of Droplet Size Distributions of Meshes Used in Validation 2 With Experimental Data of Anderson et al. [Anderson, Ryan, Santoro, and Hewitt, 1995]

findings of Arienti et al. [Arienti, Li, Soteriou, Eckett, Sussman, and Jensen, 2013], the use of the intermediate (M5) and fine (M6) meshes seems to have improved the computational accuracy compared to the coarse mesh (M4) in terms of droplet size. On the other hand, the difference observed in the number of droplets between the experiment and case M6 could be due to the relatively shorter run time of this case compared to the other two cases.

Table 4: Comparison of D10 Results With Experimental Data of Anderson et al. [Anderson, Ryan, Pal, and Santoro, 1992]

	Experiment	**M4**	**M5**	**M6**
D10 (μm)	182.3	212.2	185.3	172
Difference (%)		16.4	1.6	5.7

Table 4 shows the comparison of the mean droplet diameter (D10) predicted in simulations with the experimental data given in the study of Anderson et al. [Anderson, Ryan, Pal, and Santoro, 1992]. Both the experimental and numerical values shown in Table 4 were acquired at 16 mm below the impingement point. In the current study, an average of the droplet diameters was calculated using different time intervals until the end of an analysis. The percentage differences given are calculated with respect to the experimental data. The accuracy of the predictions clearly improves in simulations M5 and M6 compared to M4.

CONCLUSION

In this study, numerical computations are conducted to analyze the spray characteristics of a doublet injector using ANSYS Fluent 17.0 using the CLSVOF method and the AMR technique. The computational methodology is validated using two sets of experimental data from literature that were presented in terms of droplet sizes. A range of minimum cell sizes is considered for mesh sensitivity studies by taking into account the other findings in literature as well as the limited computational resources that were available at the time of the study. The predictions obtained with the use of minimum mesh cell sizes of 40 μm and 30 μm are found to be in agreement with experiments by about 11% and 4% on average in the two validation studies presented. These two cell sizes also produce results in close agreement with each other and are observed to resolve the known liquid sheet characteristics such as the liquid core, surface waves, ligaments, holes, and droplets when compared to the other cell sizes examined in the current study. Comparisons of velocity distributions with the existing numerical results along the impingement line further show that the smaller of the two cell sizes is observed to give slightly better agreement in exchange of computational costs. Even with the other presented comparisons where many differences and lack of information were noted, the general trends of velocity distributions at selected regions seem to be still captured reasonably. In summary, it is observed that the CLSVOF method with the AMR technique can be considered to simulate the atomization process of impinging jets in doublet injectors with reasonable accuracy. A minimum cell size of 40 μm is found to provide reasonable accuracy with an acceptable computational cost. It is hoped that these findings will serve other researchers in their future computations.

ACKNOWLEDGMENTS

In this research, the High Performance Computing (HPC) resources of METU Center for Wind Energy (METUWIND) were used.

References

Anderson, W. E., Ryan, H. M., Pal, S., and Santoro, R. J. (1992) Fundamental Studies of Impinging Liquid Jets. *30th Aerospace Sciences Meeting & Exhibit, Reno, NV, January 1992.* AIAA Paper 1992-0458.

Anderson, W.E. Ryan, H. M., Santoro, R. J., and Hewitt, R. E. (1995) Combustion Instability Mechanism in Liquid Rocket Engines Using Impinging Jet Injectors. *31st AIAA ASME SAE ASEE Joint Propulsion Conference, San Diego, CA, July 1995.* AIAA Paper 1995-2357

Arienti, M., Li, X., Soteriou, M. C., Eckett, C. A., Sussman, M., and Jensen, R. J. (2013). Coupled Level-Set/Volume-of-Fluid Method for Simulation of Injector Atomization. *Journal of Propulsion and Power*, *29*(1), pp. 147–157. https://doi.org/10.2514/1.b34198

Balasubramanian, A. K., Kumar, V., Nakod, P., Schütze, J., and Rajan, A. (2020). Multiscale Modelling of a Doublet Injector Using Hybrid Vof-Dpm Method. *AIAA Scitech 2020 Forum*. Orlando, FL, January 2020. AIAA Paper 2020-228, doi:10.2514/6.2020-2284

Chen, X., Ma, D., and Yang, V. (2012). Dynamics and Stability of Impinging Jets, *ILASS Americas, 24th Annual Conference on Liquid Atomization and Spray Systems, San Antonio, TX, May 2012*

Gill, G. S., Nurick, W. H., Keller, R. B., Douglass, H. W., (1976). Liquid Rocket Engine Injectors (pp. 2-18, Publication No. NASA SP-8089). Cleveland, Ohio: National Aeronautics and Space Administration, Lewis Research Center.

Huzel, D. K. and Huang, D. H. (1992). Chapter 4.5: Injector Design. In *Modern Engineering for Design of Liquid-Propellant Rocket Engines* (Vol. 147, pp. 105-115). SW, Washington DC: American Institute of Aeronautics and Astronautics.

Lai, W., Huang, W., and Chu, C. (2004). Atomization and Mixing Characteristics of an Unlike-Doublet Impinging-Jet Spray. *International Journal of Turbo and Jet Engines, 21*(2), pp.127-133, doi:10.1515/tjj.2004.21.2.127

Ryan, H. M., Anderson, W. E., Pal, S., and Santoro, R. J. (1995). Atomization Characteristics of Impinging Liquid Jets. *Journal of Propulsion and Power, 11*(1), pp.135-145. doi:10.2514/3.23851

Sussman, M., Smith, K., Hussaini, M., Ohta, M., and Zhi-Wei, R. (2007). A Sharp Interface Method for Incompressible Two-Phase Flows. *Journal of Computational Physics, 221*(2), pp. 469-505. doi:10.1016/j.jcp.2006.06.020

Wang, Z. (2016). Chapter 2.4: Atomization Modeling for Liquid Rocket Engine Atomizers. In *Internal Combustion Processes of Liquid Rocket Engines* (pp. 59-75). Singapore: John Wiley & Sons Singapore Pte.

Zheng, G., Nie, W., Feng, S., and Wu, G. (2015). Numerical Simulation of the Atomization Process of a Like-Doublet Impinging Rocket Injector. *Procedia Engineering, 99*, pp. 930-938. doi:10.1016/j.proeng.2014.12.624